SUPPORTING INFORMATION

Deactivation of Sn-Beta Zeolites Caused by Structural Transformation of Hydrophobic to Hydrophilic Micropores during Aqueous-Phase Glucose Isomerization

Michael J. Cordon[1], Jacklyn N. Hall[1], James W. Harris[1], Jason S. Bates,[1] Son-Jong Hwang,[2] Rajamani Gounder[1,*]

[1]*Charles D. Davidson School of Chemical Engineering, Purdue University, 480 Stadium Mall Drive, West Lafayette, IN 47907, USA*

[2]*Chemical Engineering, California Institute of Technology, Pasadena, CA 91101, USA*

*Corresponding author. E-mail: rgounder@purdue.edu

S.1. Bulk structural and Lewis acid site characterization of Sn-Beta zeolites

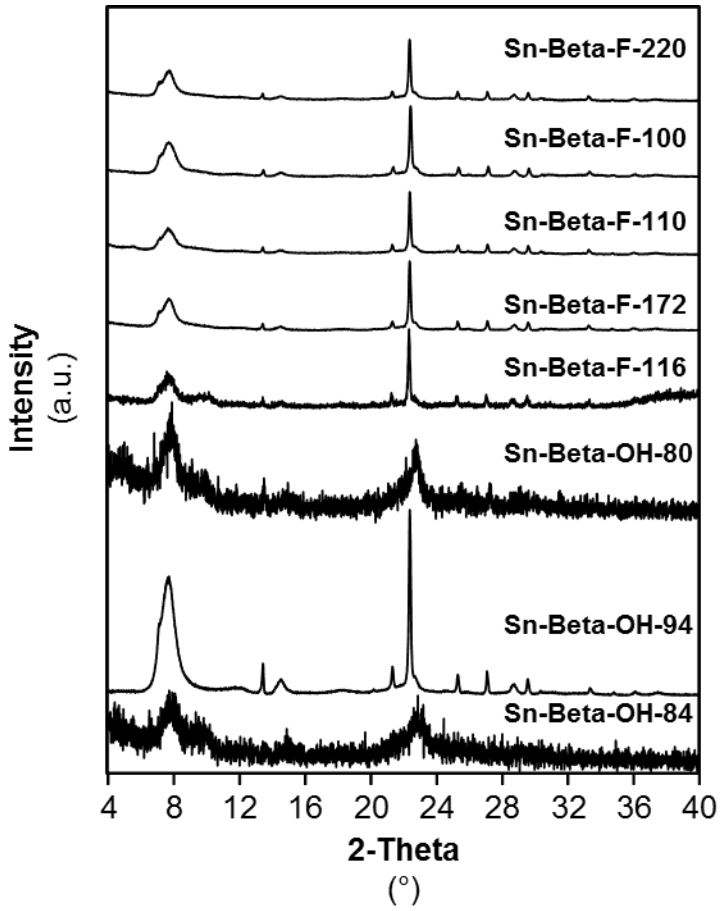

Figure S.1. Powder XRD patterns of Sn-Beta samples studied in this work.

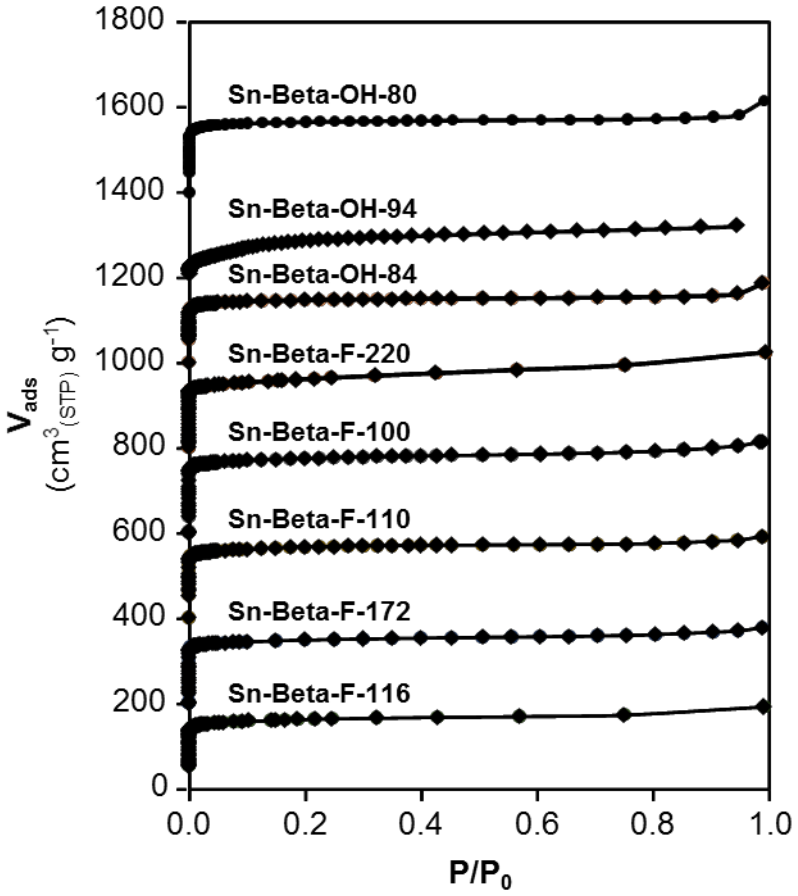

Figure S.2. N_2 adsorption isotherms (77 K) of Sn-Beta samples studied in this work. Isotherms are offset by 200 cm^3 g^{-1} for clarity.

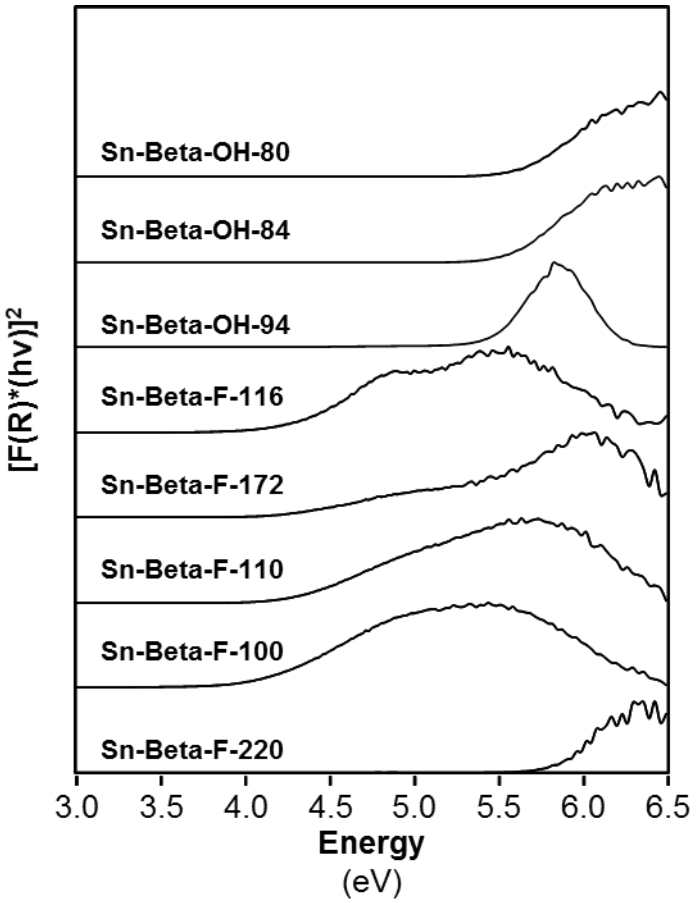

Figure S.3. Tauc plots of Sn-Beta samples studied in this work after treatment in flowing He at 523 K for 1800 s. Edge energies are summarized in Table 1.

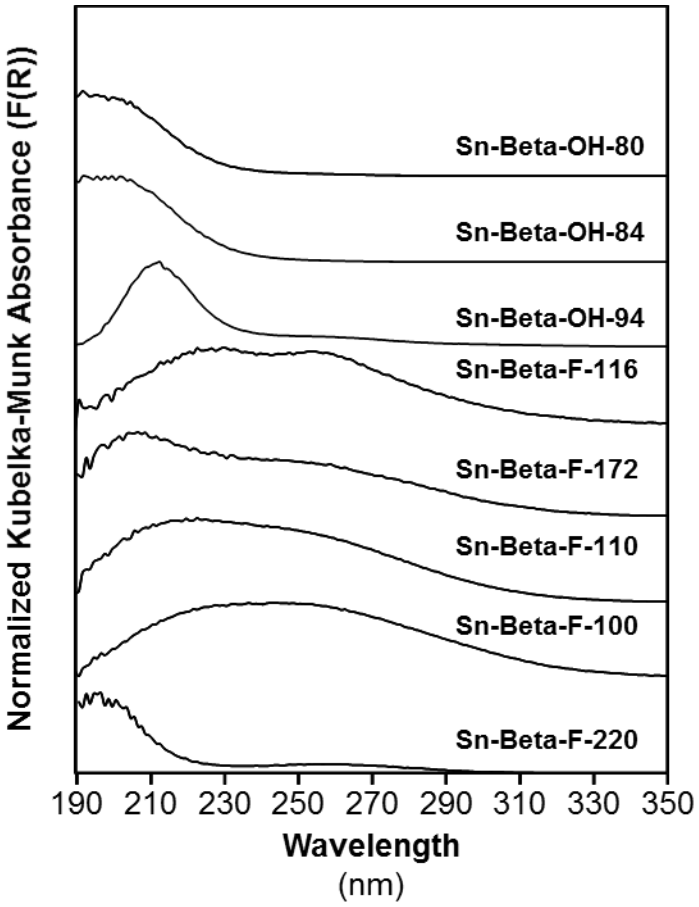

Figure S.4. Dehydrated UV-Vis spectra (523 K, 1800 s) of Sn-Beta samples studied in this work.

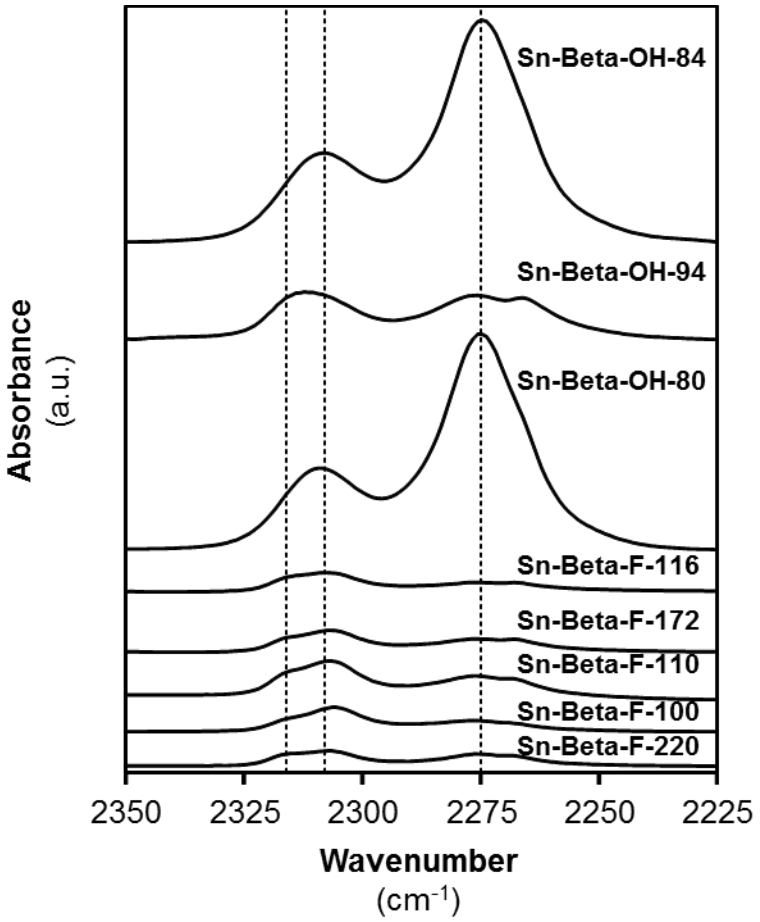

Figure S.5. IR spectra collected on CD_3CN-saturated Sn-Beta samples studied in this work. Spectra were normalized by combination and overtone modes for Si-O—Si stretches prior to the subtraction of spectra collected before CDCN adsorption. Dashed lines are drawn at 2308 cm^{-1} (CD_3CN bound to closed Sn), 2316 cm^{-1} (CD_3CN bound to open Sn), and 2275 cm^{-1} (CD_3CN bound to silanols).

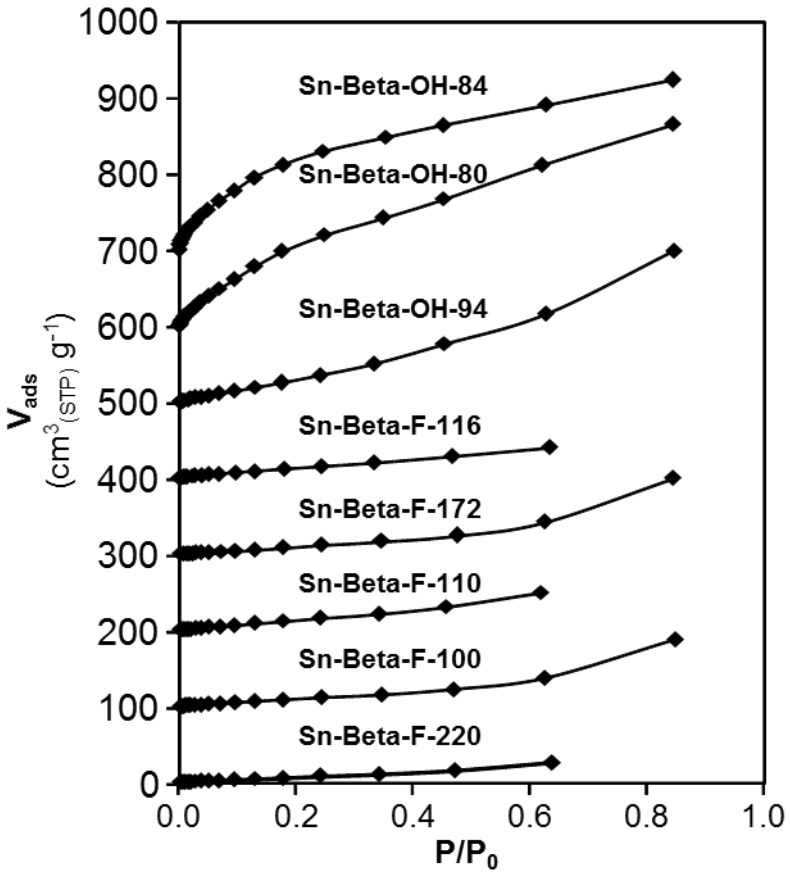

Figure S.6. Vapor-phase water adsorption isotherms (293 K) on Sn-Beta samples studied in this work. Isotherms are offset by 100 cm^3 g^{-1} for clarity.

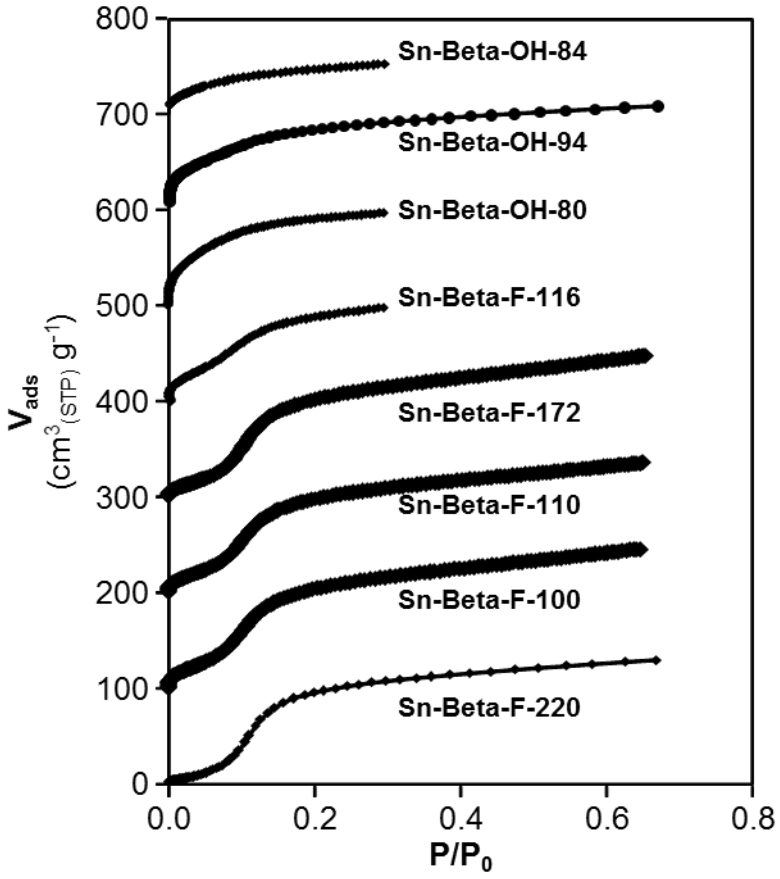

Figure S.7. Vapor-phase methanol adsorption isotherms (293 K) on Sn-Beta samples studied in this work. Isotherms are offset by 100 cm^3 g^{-1} for clarity.

S.2. Rate constant and free energy measurements on Sn-Beta samples

Apparent first-order glucose-fructose isomerization rate constants (1-10 wt% glucose) measured on Sn-Beta samples free energy differences between 1,2-hydride shift transition states and two water molecules bound to the Lewis acidic Sn site, the most abundant reactive intermediate (MARI) under aqueous-phase operating conditions [1]. The ~3x difference in first-order rate constants (normalized per open Sn site) reflect small free energy differences (~3 kJ mol^{-1}) between the kinetically-relevant transition state and the reference state comprising two bound water ligands at the Sn site. Thus, activation and deactivation phenomena reflect free energy decreases and increases, respectively, which are distinct from the 3 kJ mol^{-1} differences between individual samples.

S.3. Bulk characterization of Sn-Beta-F-116 after controlled hot (373 K) water exposure

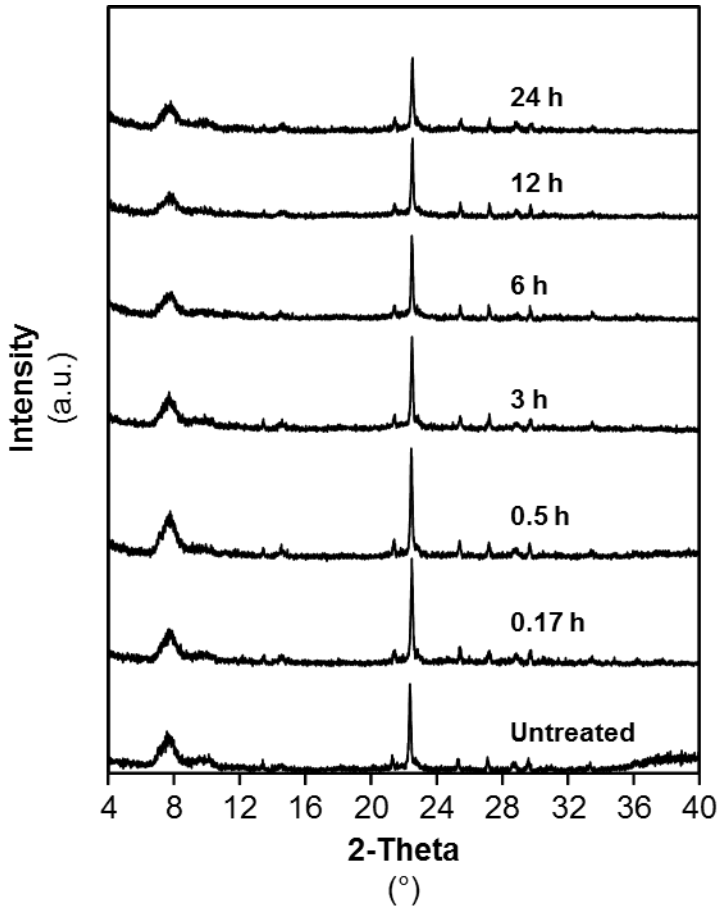

Figure S.8. Powder XRD patterns of Sn-Beta-F-116 samples after various (0-24 h) amounts of hot (373 K) water exposure time.

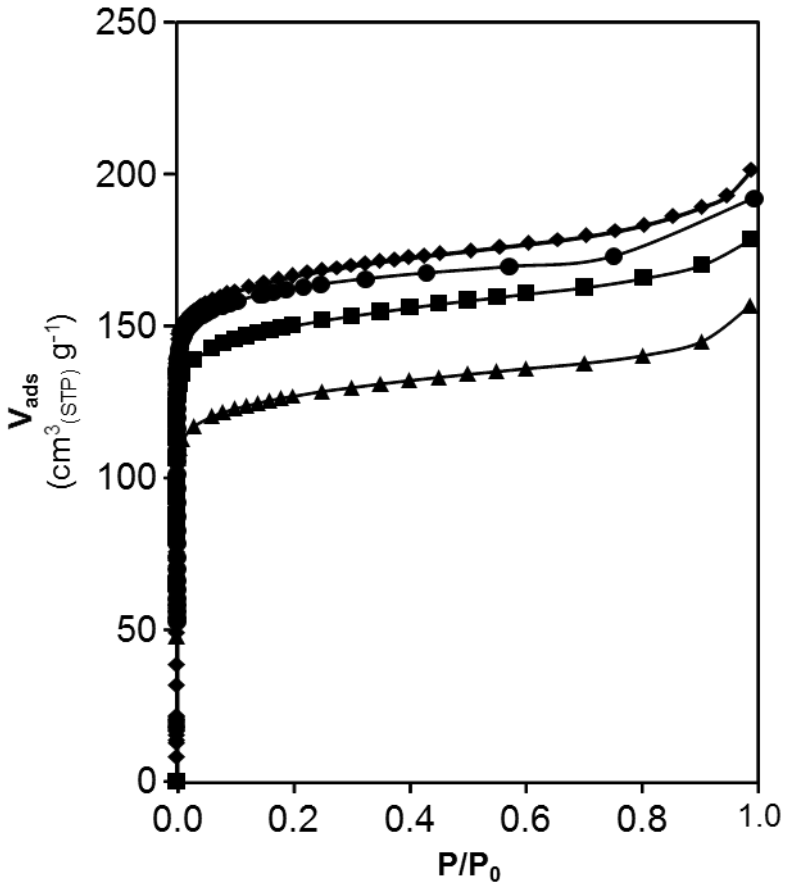

Figure S.9. N_2 adsorption isotherms (77 K) of Sn-Beta-F-116 after 0 (diamond), 0.5 (circle), 3 (square), and 24 h (triangle) of hot (373 K) water exposure time.

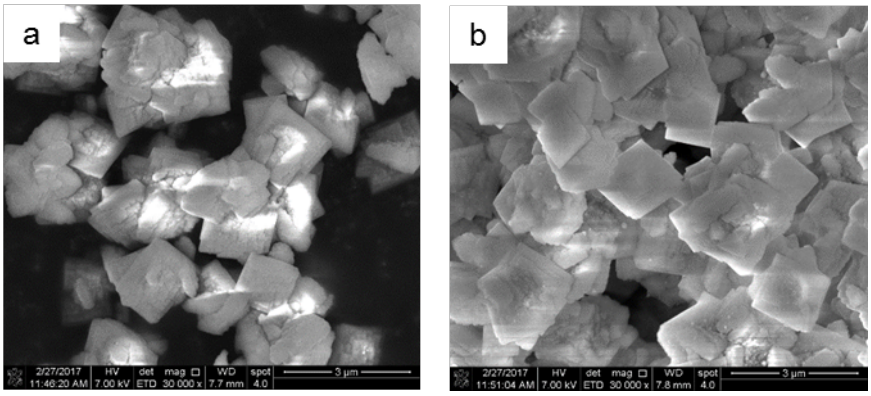

Figure S.10. SEM images of Sn-Beta-F-116 (a) before and (b) after 24 h of hot (373 K) water exposure time.

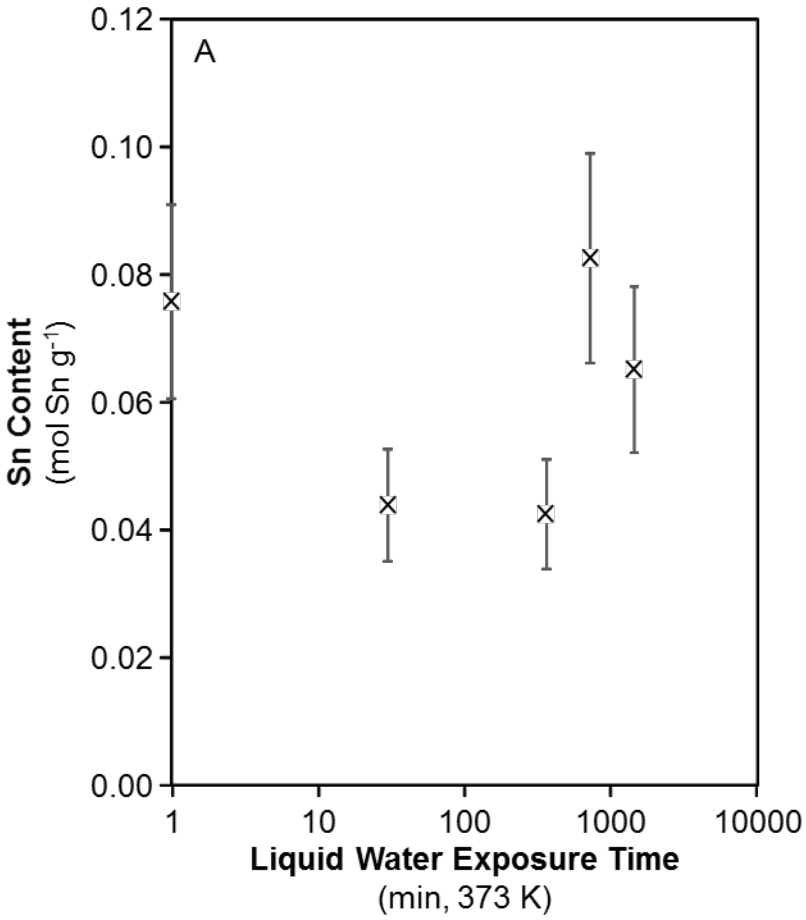
A
0.12
0.10
0.08
0.06
0.04
0.02
0.00
Sn Content
(mol Sn g-1)
1
10
100
1000
10000
Liquid Water Exposure Time
(min, 373 K)

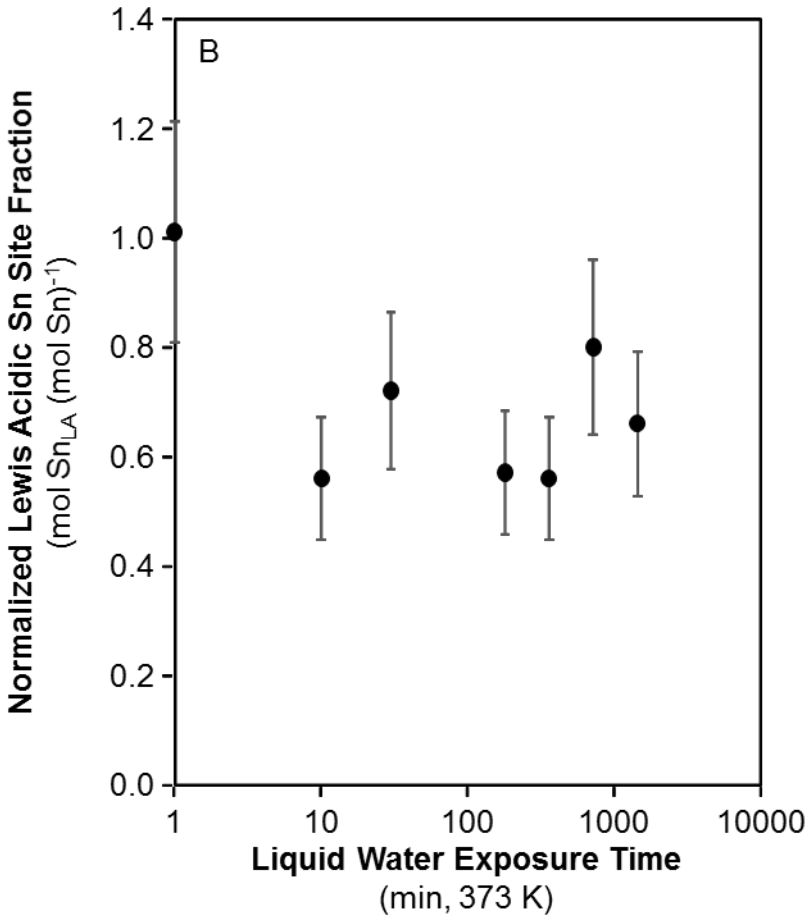
B
1.4
1.2
1.0
0.8
0.6
0.4
0.2
0.0
Normalized Lewis Acidic Sn Site Fraction
(mol Sn$_{LA}$ (mol Sn)$^{-1}$)
1
10
100
1000
10000
Liquid Water Exposure Time
(min, 373 K)

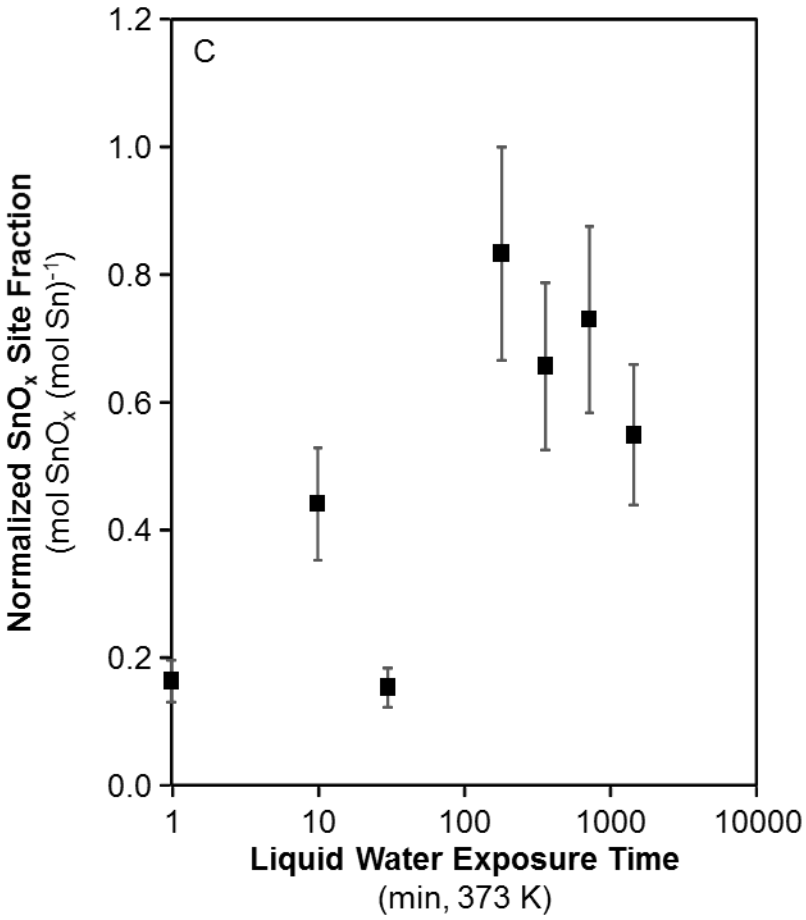

Figure S.11. Sn density (A), Lewis acidic Sn fraction (B), and SnO_x fraction (C) on Sn-Beta-F-116 as a function of liquid water exposure time. Site densities on untreated materials are plotted at 1 min of water exposure.

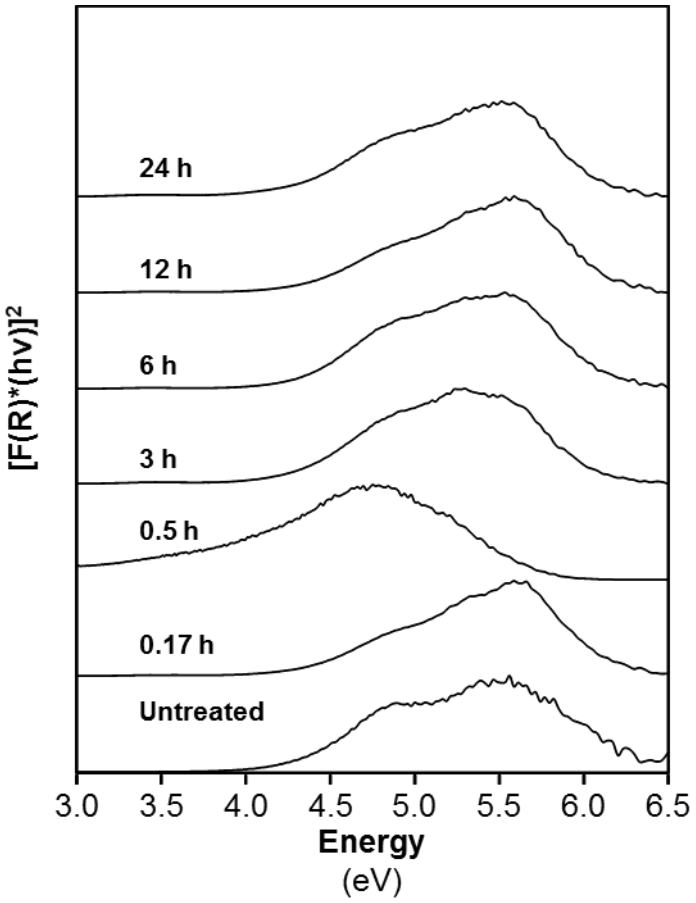

Figure S.12. Tauc plots collected after treatment in flowing He at 523 K for 1800 s on Sn-Beta samples after various (0-24 h) amounts of hot (373 K) water exposure time.

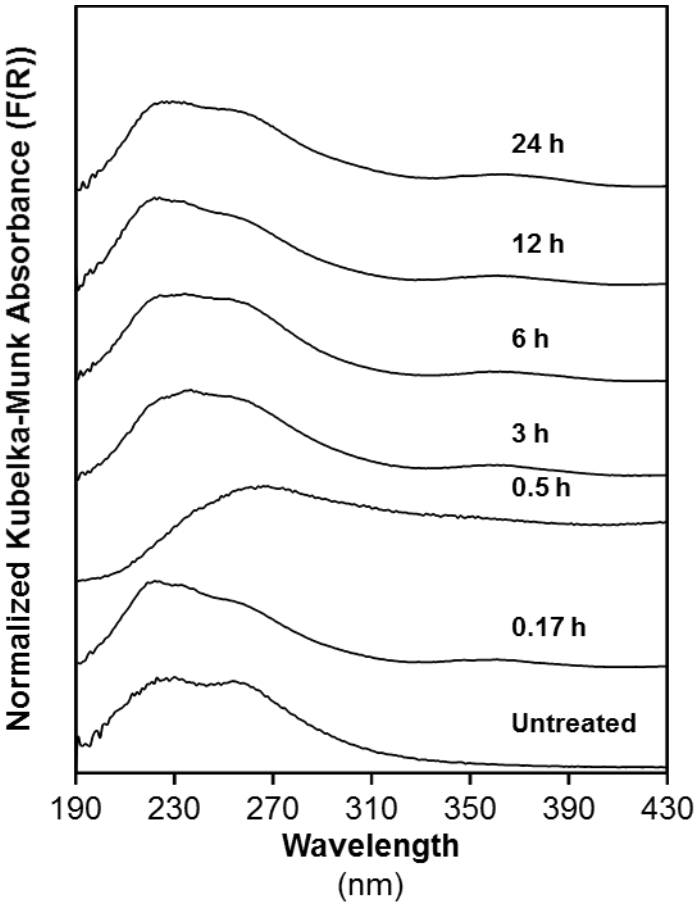

Figure S.13. Dehydrated UV-Vis spectra (523 K, 1800 s) of Sn-Beta samples after various (0-24 h) amounts of hot (373 K) water exposure time.

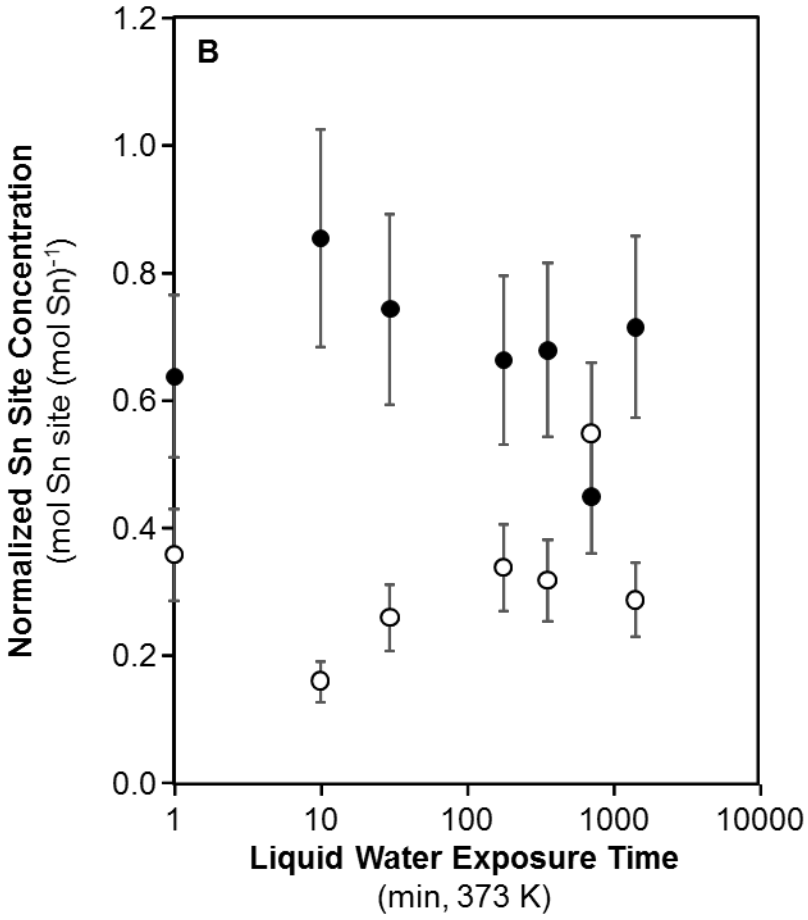

Figure S.14. Open (○) and closed Sn density (●) per mol Lewis acidic Sn on Sn-Beta-F-116 as a function of liquid water exposure time. Site densities on untreated materials are plotted at 1 min of water exposure.

S.4. Bulk characterization of Sn-Beta-F-100 after NMe_4OH treatment

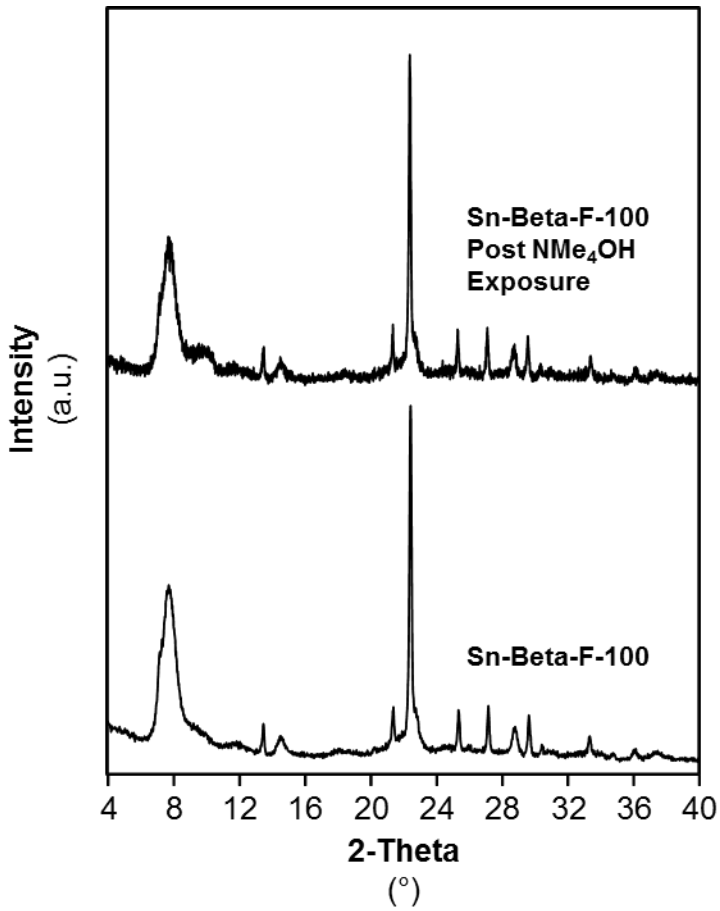

Figure S.15. Powder XRD patterns of Sn-Beta-F-100 samples before and after NMe_4OH treatment.

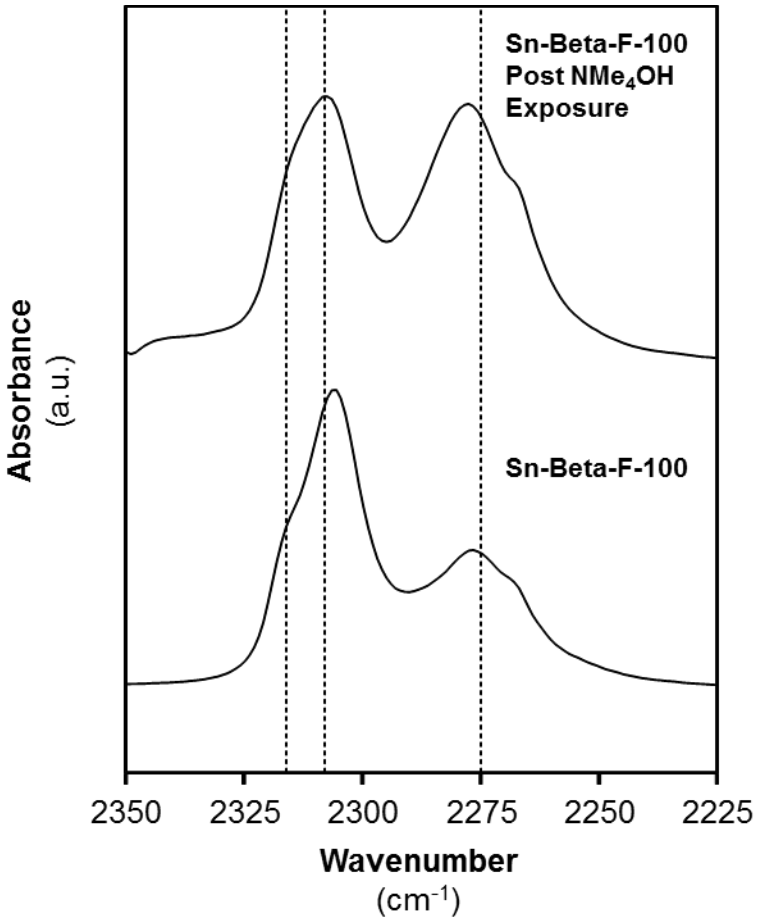

Figure S.16. IR spectra collected on CD_3CN-saturated Sn-Beta-F-100 samples before and after NMe_4OH treatment. Spectra were normalized by combination and overtone modes for Si-O—Si stretches prior to the subtraction of spectra collected before CDCN adsorption. Dashed lines are drawn at 2308 cm^{-1} (CD_3CN bound to closed Sn), 2316 cm^{-1} (CD_3CN bound to open Sn), and 2275 cm^{-1} (CD_3CN bound to silanols).

S.5. Supplemental figures on kinetic and mechanistic details of activation and fructose formation on Sn-Beta samples

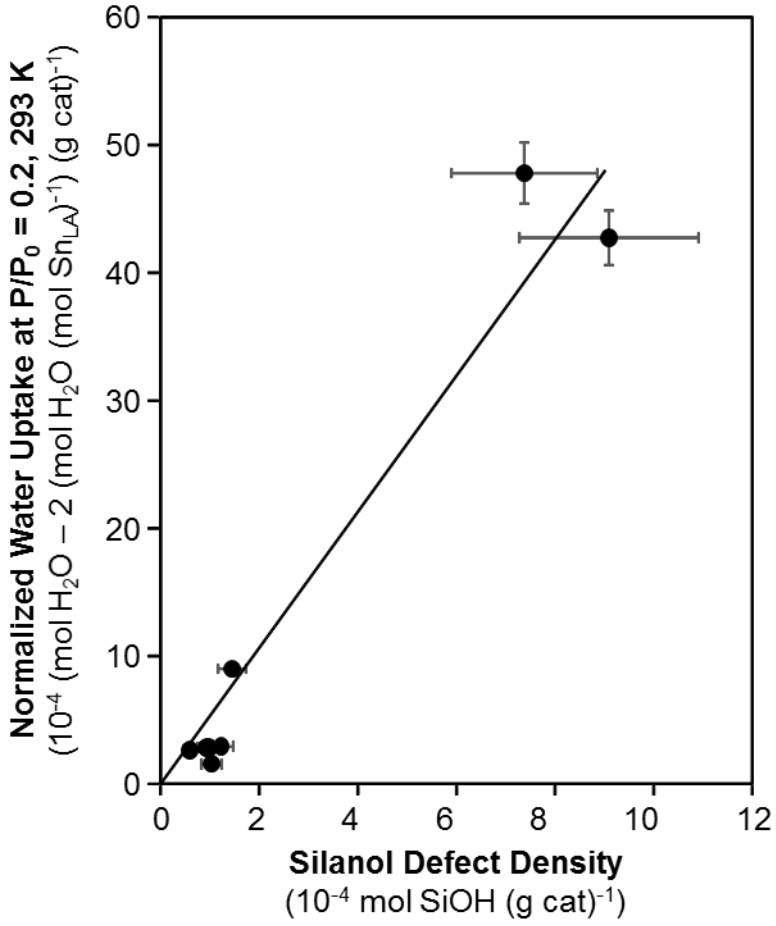

Figure S.17. Water uptakes at P/P_0 = 0.2 (373 K) after rigorously subtracting off two water molecules per Lewis acid site counted from CD_3CN titration plotted against bulk silanol defect density from CD_3CN titration measurements. The solid line is a best fit line forced through the origin to guide the eye.

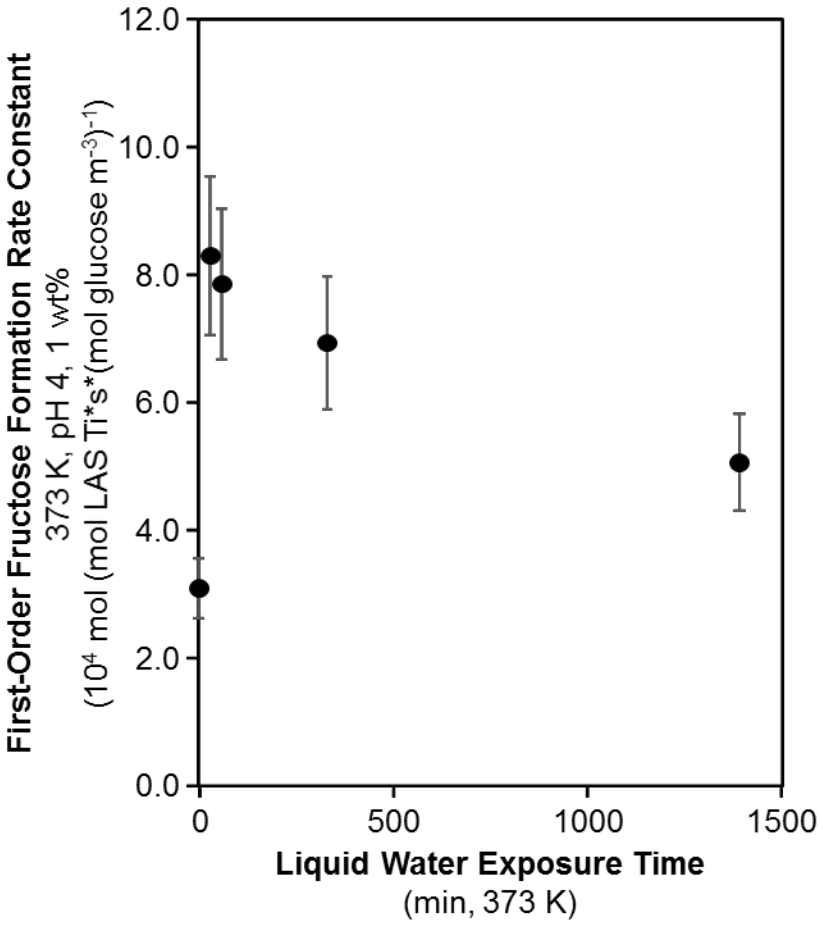

Figure S.18. Measured first-order glucose isomerization rates (per Lewis acidic Ti, 373 K) on Ti-Beta-F-155 after hot (373 K) liquid water exposure (0-24 h). Characterization data on Ti-Beta-F-155 is reported in Ref. [2].

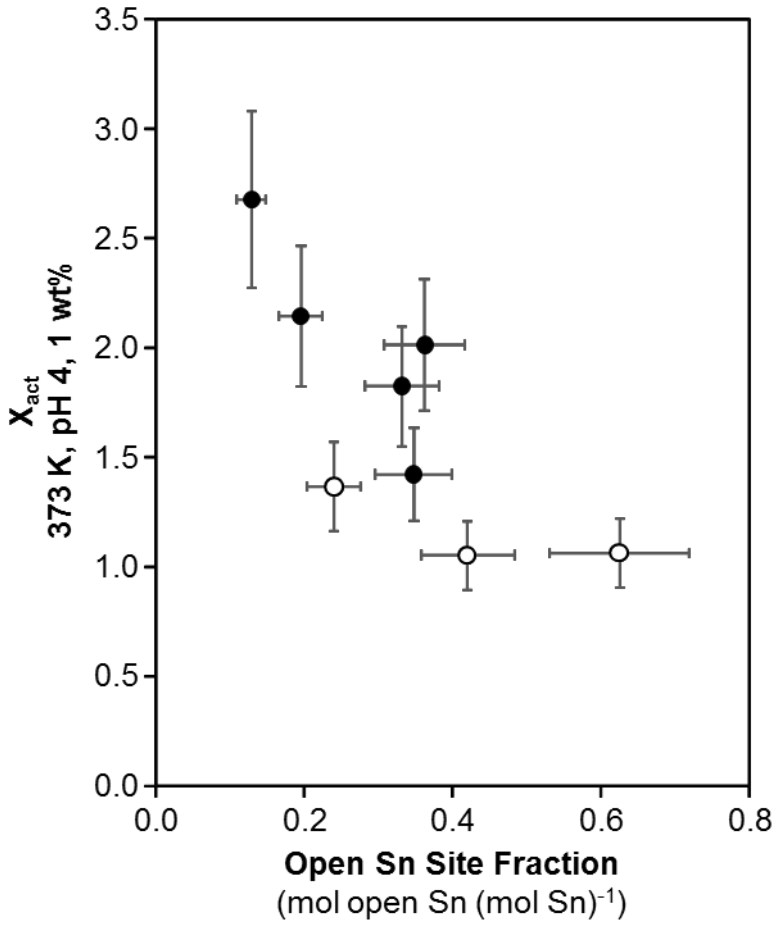

Figure S.19. Observed activation extents (373 K, 1 wt%) as a function of initial open Sn density on Sn-Beta-F (closed) and Sn-Beta-OH (open) zeolites. Observed activation extents are defined as the ratio of the highest measured first-order glucose isomerization rate constant per sample normalized by the measured first-order rate constant on the unexposed Sn-Beta sample.

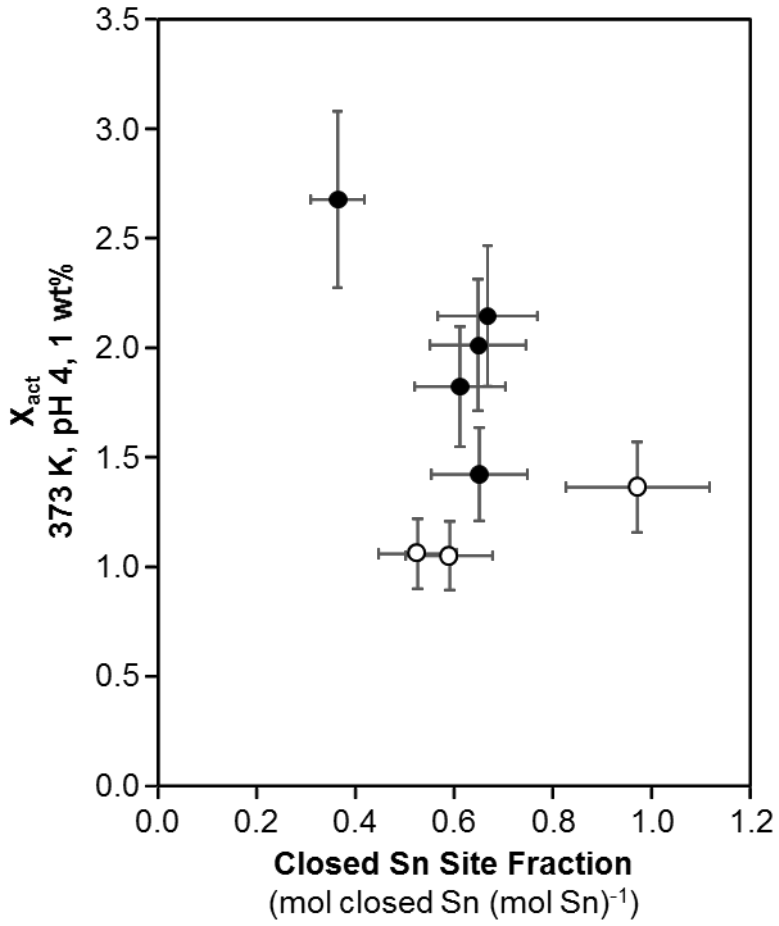

Figure S.20. Observed activation extents (373 K, 1 wt%) as a function of initial closed Sn density on Sn-Beta-F (closed) and Sn-Beta-OH (open) zeolites. Observed activation extents are defined as the ratio of the highest measured first-order glucose isomerization rate constant per sample normalized by the measured first-order rate constant on the unexposed Sn-Beta sample.

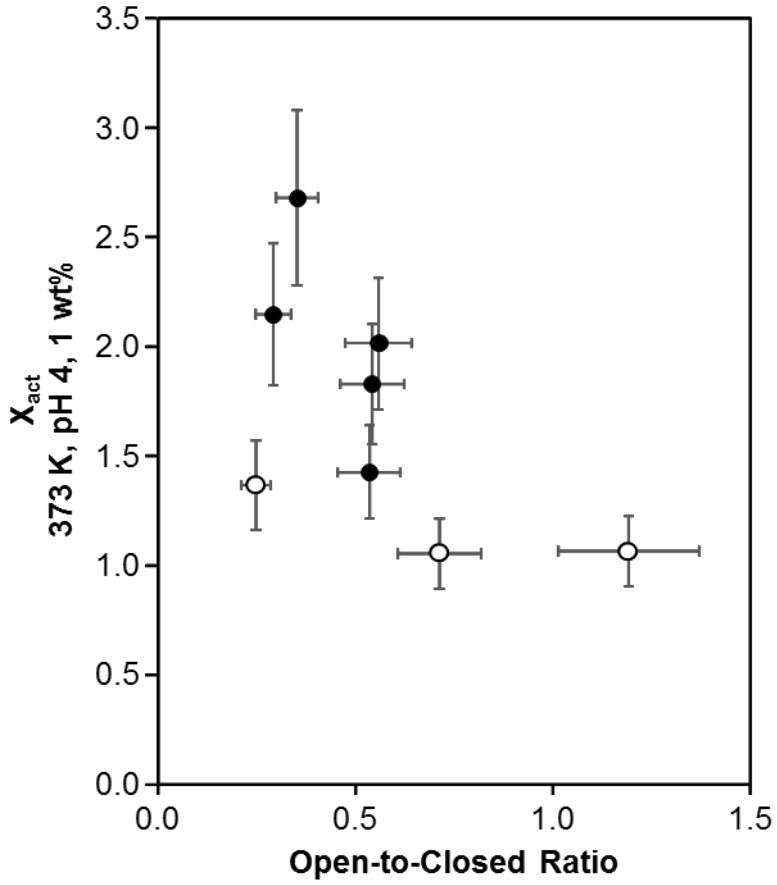

Figure S.21. Observed activation extents (373 K, 1 wt%) as a function of initial initial open-to-closed ratio on Sn-Beta-F (closed) and Sn-Beta-OH (open) zeolites. Observed activation extents are defined as the ratio of the highest measured first-order glucose isomerization rate constant per sample normalized by the measured first-order rate constant on the unexposed Sn-Beta sample.

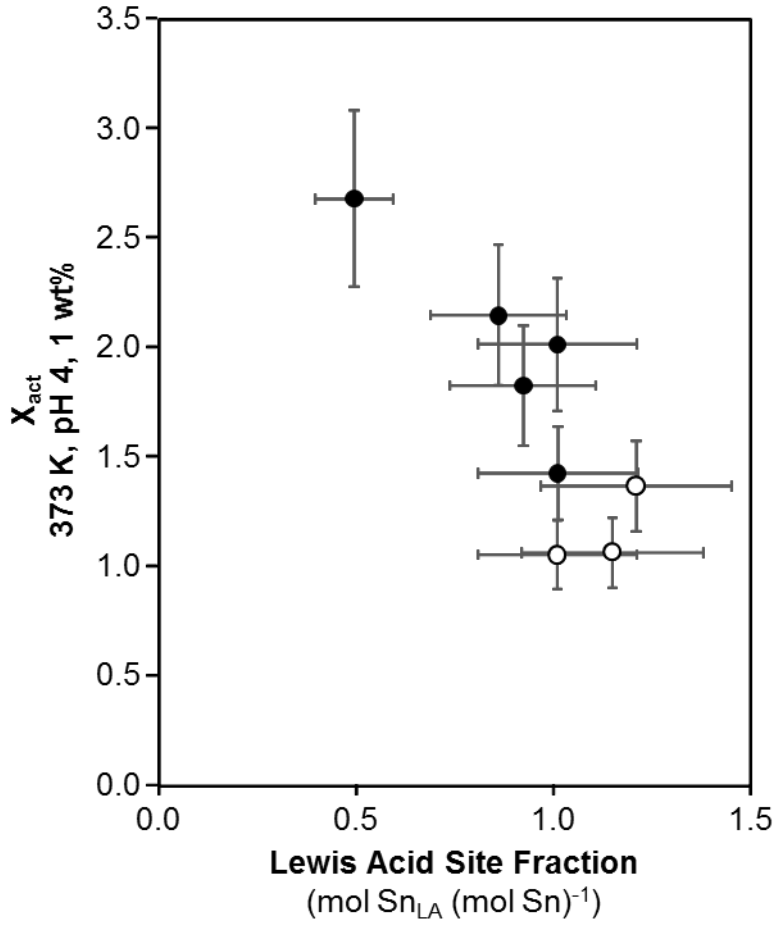

Figure S.22. Observed activation extents (373 K, 1 wt%) as a function of initial Lewis acidic Sn density on Sn-Beta-F (closed) and Sn-Beta-OH (open) zeolites. Observed activation extents are defined as the ratio of the highest measured first-order glucose isomerization rate constant per sample normalized by the measured first-order rate constant on the unexposed Sn-Beta sample.

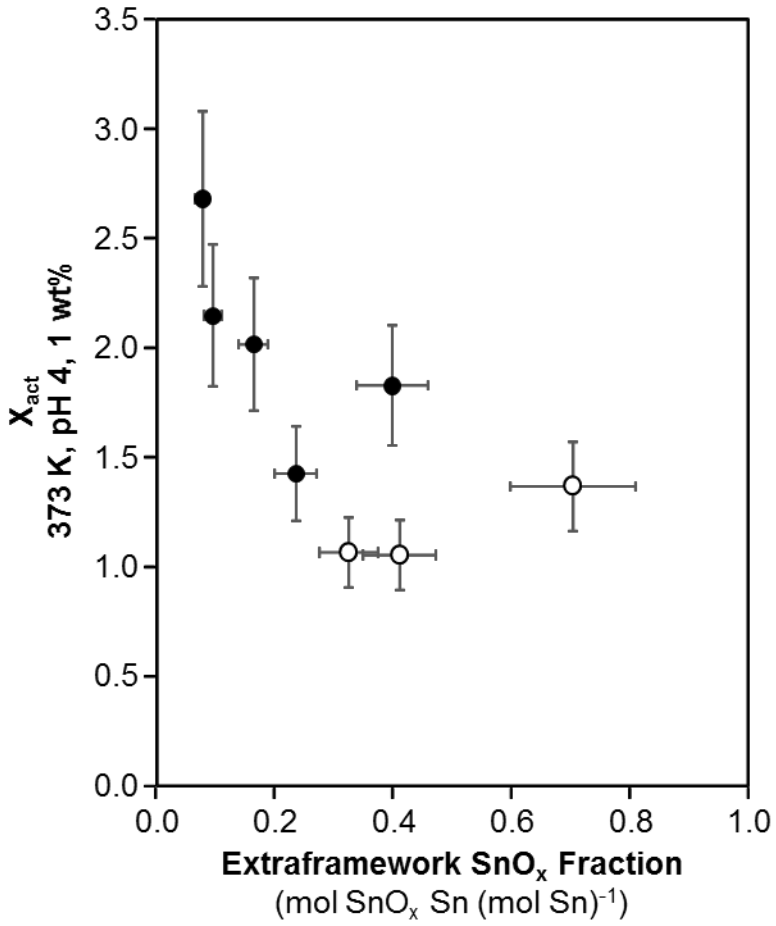

Figure S.23. Observed activation extents (373 K, 1 wt%) as a function of initial SnO_x density on Sn-Beta-F (closed) and Sn-Beta-OH (open) zeolites. Observed activation extents are defined as the ratio of the highest measured first-order glucose isomerization rate constant per sample normalized by the measured first-order rate constant on the unexposed Sn-Beta sample.

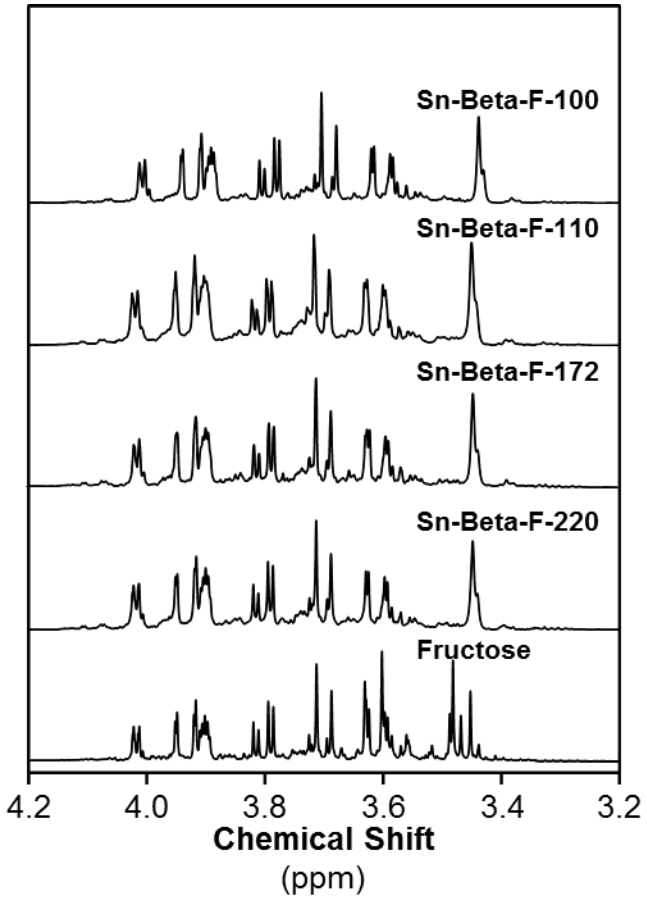

Figure S.24. Solution-phase ^{1}H NMR of fructose products formed after contacting 1 wt% glucose solutions (373 K) with Sn-Beta-F samples. A fructose standard is given for direct comparison.

References

[1] J.W. Harris, M.J. Cordon, J.R. Di Iorio, J.C. Vega-Vila, F.H. Ribeiro, R. Gounder, Titration and quantification of open and closed Lewis acid sites in Sn-Beta zeolites that catalyze glucose isomerization, Journal of Catalysis, 335 (2016) 141-154.
[2] M.J. Cordon, J.W. Harris, J.C. Vega-Vila, J.S. Bates, S. Kaur, M. Gupta, M.E. Witzke, E.C. Wegener, J.T. Miller, D.W. Flaherty, D.D. Hibbitts, R. Gounder, Dominant Role of Entropy in Stabilizing Sugar Isomerization Transition States within Hydrophobic Zeolite Pores, Journal of the American Chemical Society, 140 (2018) 14244-14266.